35th Annual International Conference of the IEEE EMBS
Osaka, Japan, 3 - 7 July, 2013

# Computer-Aided Diagnosis in Endoscopy: A Novel Application Toward Automatic Detection of Abnormal Lesions on Magnifying Narrow-Band Imaging Endoscopy in the Stomach

Tsung-Chun Lee, MD (Member IEEE)[1], Yu-Huei Lin[2], Noriya Uedo, MD[3], Hsiu-Po Wang, MD[1], Hsuan-Ting Chang, PhD (Senior Member IEEE)[2], Chung-Wen Hung PhD (Member IEEE)[2]

***Abstract*—**Gastric cancer is the fourth common cancer and the second major cause of cancer death worldwide. Early detection of gastric cancer by endoscopy surveillance is actively investigated to improve patient survival, especially using the newly developed magnifying narrow-band imaging endoscopy in the stomach. However, meticulous examination of the aforementioned images is both time and experience demanding and interpretation could be variable among different doctors, which hindered its widespread application. In this study, we developed a new image analysis system by adopting local binary pattern and vector quantization to perform pattern comparison between known training abnormal images and testing images of magnifying narrow band endoscopy images in the stomach. Our preliminary results demonstrated promising potential for automatically labeled region of interest for endoscopy doctors to focus on abnormal lesions for subsequent targeted biopsy, with the rates of recall 0.46-1.00 and precision 0.39-0.87.

## I. Introduction

Gastric cancer is the fourth common cancer worldwide and is also the second major cause of cancer death. Early detection and prompt treatment remain the best measure to improve patient survival. Recent advance in endoscopy technologies including magnification and narrow-band imaging (NBI) offers a new tool for clinical doctors to early detect abnormal lesions in the stomach by demonstrating abnormal mucosal surface morphologies. However, current practice of endoscopy magnification and NBI relies heavily on clinical doctors' own experiences and meticulous examination of each frame of magnified images in the whole stomach can be very time-consuming. Furthermore, there could be significant interpersonal variability in the performance of endoscopy diagnosis between different endoscopy doctors.

In this study, we aim to develop computer-aided diagnosis algorithms in endoscopy for automatic detection of high-risk lesions on the magnified endoscopy images, thereby reducing the variability and enhancing the efficiency in diagnosis. We adopted image features of mucosal surface vasculature and surface structures, including tortuosity, dilatation, metamorphosis, fuzziness, light blue crest and microvasculature, according to [1]. We analyzed these image features using image analysis algorithms and the final output of currently developed algorithms would be providing an automatically labeled "region of interest" (auto-ROI) for clinical doctors to constitute further investigations such as targeted biopsy.

[1]Department of Internal Medicine, National Taiwan University Hospital and College of Medicine, National Taiwan University, Taipei, Taiwan; [2]Department of Electrical Engineering, National Yunlin University of Science and Technology, Yunlin, Taiwan; [3]Department of Gastrointestinal Oncology, Osaka Medical Center for Cancer and Cardiovascular Diseases, Higashinari-ku, Osaka, Japan

### A. Study Materials: Magnifying Narrow Band Imaging Endoscopy Images in the Stomach

Ezoe *et. al.* [2] indicated that magnifying NBI, as compared with conventional white light imaging, provided better accuracy, sensitivity, and specificity in detection of early gastric cancer. We obtained study materials (27 images of abnormal lesions and 30 normal images) from our collaborator researcher (Dr. Noriya Uedo), who is an expert endoscopy doctor in magnifying NBI in the stomach. We stored the magnifying NBI images as 639×480 bmp files.

### B. Image Features

We aim to develop an automatically labeled ROI (auto-ROI) to facilitate clinical endoscopy doctors who can then do necessary targeted biopsy. We adopted the image features of tortuosity, dilatation, metamorphosis, fuzziness, light blue crest, and microvasculature, according to [1, 9]. These image features were clinically utilized by clinical endoscopy doctors to determine suspicious pathological area under magnifying NBI endoscopy.

### C. Vector Quantization

We utilized the method of "Vector Quantization (VQ)," which is originally used to efficiently compress the images as indices of code vectors in a pre-designed codebook. We separated the original image to $w \times w$ sub-images, which are segmented image blocks and can be represented as multi-dimensional vectors. Given an input image, the segmented image blocks can be coded by using the indices of the most similar code vectors to represent the whole sub-images.

In this study, we exploited the unique compression feature of VQ to markedly reduce the data volume of codebook. We also utilized representative "Local Binary Pattern (LBP)" algorithm to reduce the computation complexity and time consumption in pattern comparison.

There are usually three common methods in the generation of a codebook: K-mean algorithm, Linde-Buzo-Gray (LBG) algorithm, and centroid splitting algorithm. We adopted K-mean algorithm [3] in this study.

According to the quantization number $k$, we randomly assign $k$ numbers of center points, $\{c_1(h), c_2(h), \dots, c_k(h)\}$, where $h$ means the $h^{\text{th}}$ learning cycle. We also sorted training samples according to the following formula:

$$z_n \in Q_j(h) \text{ if } \left\|z_n - c_j(h)\right\| < \left\|z_n - c_i(h)\right\|$$

978-1-4577-0216-7/13/$26.00 ©2013 IEEE

$$\text{for all } i = 1,2,\dots,k. \quad i \neq j, \tag{1}$$

where $Q_j(h)$: the $j^{\text{th}}$ subgroup in the $h^{\text{th}}$ learning cycle and $z_n$ denotes the input patterns to VQ. Then, the new converging center point is calculated again:

$$c_j(h+1) = \frac{1}{M_j}\sum_{z_n \in Q_j(h)} z_n, \tag{2}$$

where $M_j$ is the sample size of $Q_j$. The above calculation process continues until the full convergence is obtained.

## II. METHOD

### A. Working flow of the proposed system

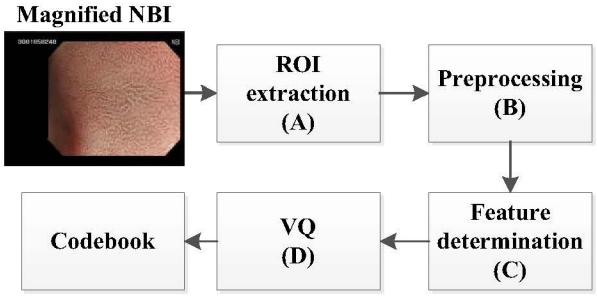


Figure 1. Block diagram for codebook generation in the proposed system

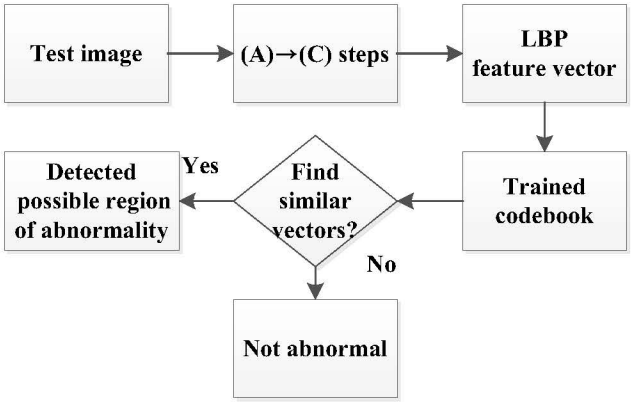


Figure 2. Block diagram for testing images and defining possible area of abnormality (ROI) in the proposed system

We selected ROIs from the original magnified NBI images in the stomach. The selection of ROIs in each image was made by an experienced endoscopy doctor (T.-C. L). We perform the preprocessing of ROI and then the feature determination. Because the quantity of image parameters is huge, we adopted VQ on the image features to compress the image data, in order to reduce the computation complexity. In total, we examined 27 images of abnormal lesions and 30 normal images.

### B. Region of Interest extraction

In this study, we defined an ROI area of 400×355 pixels, which exclude the black regions in the four corners of the original image, to label the abnormal lesions.

### C. Preprocessing

Before the training and testing stages, we performed preprocessing to all ROIs. Because the endoscopy images did not have uniform light distribution on the original images, variable light exposure and uneven shadow could interfere our analysis and pattern comparison between abnormal and normal part of the images. Hence we performed the mean removal method to all ROIs.

$$A(i,j) = \frac{\sum_{k=0}^{d}\sum_{l=0}^{d} I(i+k,j+l)}{(d_1+1)(d_2+1)}, \tag{3}$$

$$I'(i,j) = I(i,j) - A(i,j). \tag{4}$$

$A$: the average pixel value in the block.
$I$: each pixel in original block.
$I'$: the original pixel value ($I$) minus the average pixel value ($A$).
$d_1$、$d_2$: sizes of block, in this study $d_1$=$d_2$= $w$ (sub-images).

After the mean removal process, the images could still preserve texture features but reduce the background interference.

### D. Grayscale and Rotation Invariant Local Binary Patterns

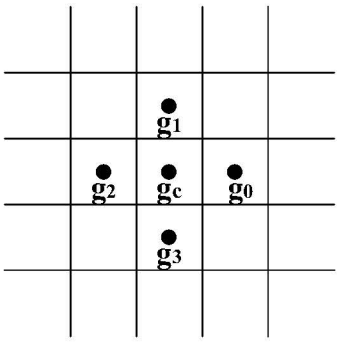


Figure 3. Circularly symmetric neighbor sets for different ($P$, $R$) combinations

Local binary patterns (LBPs) are extensively applied in many image processing tasks due to its unique capability in deciphering local texture features [4]. We first transform color images into grayscale ones and then rotate unaltered texture calculation $T$ in its joint distribution under the grayscale value of $P$ ($P$>1).

$$T = t(g_c, g_{c0}, \dots, g_{P-1}), \tag{5}$$

where $g_c$ is the grayscale value of central pixel, $g_p(p = 0,\dots,P-1)$ is the spatial pixel of circle with a radius of $R$ ($R$>0), thereby generating a circular symmetric spatial set as shown in Fig. 3, whose coordinates can be represented as $(-\mathrm{R}\sin\left(\frac{2\pi p}{P}\right), \mathrm{R}\cos\left(\frac{2\pi p}{P}\right))$.

Let $LBP_{P,R}$ denote the spatial structure of local image textures.

$$LBP_{P,R}(x,y) = \sum_{P=0}^{P-1} s(g_P - g_c)2^P \tag{6}$$

$$s(x) = \begin{cases} 1, & x \geq 1 \\ 0, & x < 0 \end{cases} \tag{7}$$

In order to fulfill rotation invariance, according to [5], we defined the "uniform" features, and we obtained "Uniform pattern".

$$LBP_{P,R}^{riu2} = \begin{cases} \sum_{p=0}^{P-1} s(g_p - g_c), & \text{if } U(LBP_{P,R}) \leq 2 \\ P+1, & \text{otherwise} \end{cases}, \tag{8}$$

where

$$U(LBP_{P,R}) = |s(g_{p-1} - g_c) - s(g_0 - g_c)| + \sum_{p=1}^{P-1} s(g_p - g_c) - s(g_{P-1} - g_c) \quad (9)$$

and $U(\cdot)$ represents the spatial transformation of its corresponding image features.

### *E. Testing set and training set*

We defined the training set ROIs after careful consultation with a clinical endoscopy doctor. Then we performed 25×25 pixel-sized rough segmentation for all training set ROIs, according to the methods in Refs. [6, 7]. Subsequently, we performed LBP calculation to each block, and recorded the determined feature vectors, up to a total number of 161,745. Because the number is huge and thus is too time-consuming in executing the pattern comparison operations, by using the way of K-means method, the feature vectors are vector-quantized to a much smaller number $K_q$,

$$K_q = 2^{round(\log_2(N))-3} \quad (10)$$

where $q \in \{1,2,3,\ldots,27\}$ is the image index and $N$ denotes the dimension of feature vector.

To obtain a testing set, we randomly selected 11 abnormal images and nine normal images. All were magnifying NBI endoscopy images in the stomach. We dissect testing images into 25×25 pixel block and performed LBP calculation. We calculated feature vectors of each block and then pairwisely compare the Euclidean distance between the testing set and training set [8].

$$D = \sqrt{\sum_{i=1}^{10} (G_i - \widehat{G_i})^2}, \quad (11)$$

where $G_i$ and $\widehat{G_i}$ denote the feature vectors of testing set and the training set, respectively.

We compared the smallest distance to the feature vector in the training set. If the smallest distance was less than 4.75, which means the testing image was "similar" (closer in the vector space) to training set (abnormal images), we then defined it as a possible area of abnormality. According to our experiments, we choose 4.75 as the best threshold value from several rounds of calculations.

## III. Experimental Results

Figures 4(a) and 4(c) showed the ROIs selected by a clinical doctor and Figure 4(b) and 4(d) showed the labeled ROIs automatically detected by the proposed system. It demonstrated that the proposed system has high potential to assist clinical endoscopy doctor in identifying possible abnormal lesions in magnified NBI images in the stomach.

Table I shows the test results of recall and precision rates for 11 test images. Both the rates vary a lot. The average recall rate is higher than the average precision rate. We obtained a recall of 0.46-1 and precision of 0.39-0.87. It appears that images with fewer blocks tended to have poor performance in both recall and precision rates. As to the standpoint of diagnosis assistance, the recall rate is more important than the precision rate.

Consider the computation complexity of the proposed method. We perform our experiments based on MATLAB coding on a PC with CPU i7-3370 and 8G-byte DRAM. The averaging processing time is around 87.5 second per test image. We understand that this is still away from real time processing. Therefore, developing a more efficient method which can accelerate the proposed method will be an important issue in our future research task.

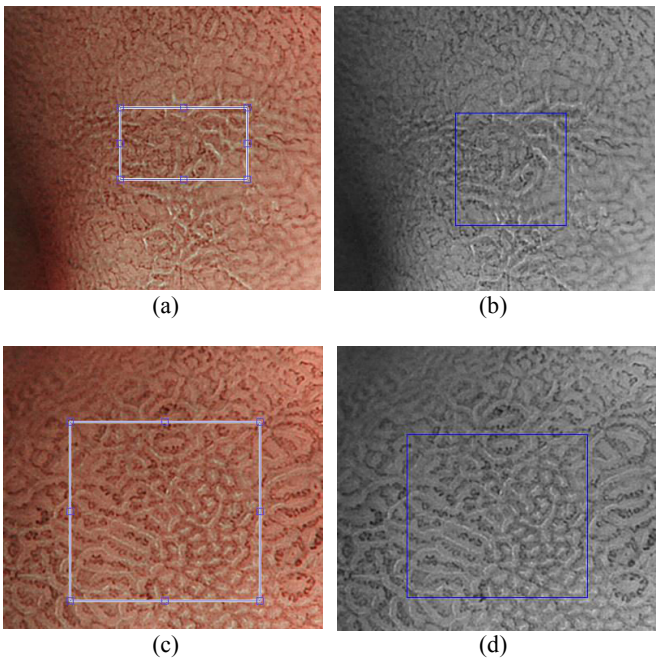

(a) (b) (c) (d)

Figure 4. automatically labeled ROIs (auto-ROI). (a) and (c): The doctor-defined ROIs; (b) and (d): the automatically labeled ROIs (auto-ROI).

TABLE I. Testing Results of Image Features

| Test Image | Abnormal lesion | Recall | Precision |
|---|---|---|---|
| Test1 | Yes | 0.77 | 0.53 |
| Test2 | Yes | 0.56 | 0.69 |
| Test3 | Yes | 0.68 | 0.72 |
| Test4 | Yes | 0.48 | 0.55 |
| Test5 | Yes | 1.00 | 0.62 |
| Test6 | Yes | 0.90 | 0.66 |
| Test7 | Yes | 0.56 | 0.87 |
| Test8 | Yes | 0.90 | 0.60 |
| Test9 | Yes | 0.71 | 0.73 |
| Test10 | Yes | 0.46 | 0.39 |
| Test11 | Yes | 0.52 | 0.47 |

## IV. CONCLUSION

Our preliminary results demonstrated feasibility of automatically labeling abnormal lesions on magnifying NBI images, in approximate location of physician-defined ROI.

This system at its current format still needs further improvement in terms of recall and precision rates. In the near future, we hope to improve the performance and achieve acceptable sensitivity and specific of our system for clinical bedside use by adding more training and testing image materials. We envision promising potential in automatically labeled ROI to facilitate clinical endoscopy doctors with real-time calculation and real-time aid in diagnosis.

## ACKNOWLEDGMENT

We would like to express gratitude for Dr. Kenshi Yao, Department of Endoscopy, Fukuoka University Chikushi Hospital, Fukuoka, Japan for his assistance in magnifying narrow band images. This research is partially supported by the National Science Council (NSC) under the contract number NSC 100-2628-E-224-002-MY2.

## REFERENCES

[1] N. Uedo, F. Mitsuhiro, G. Kenichi, "Role of narrow band imaging for diagnosis of early-stage esophagogastric cancer: current consensus of experienced endoscopists in Asia–pacific region," Digestive Endoscopy Volume 23, Issue Supplement s1,pages 58–71, May 2011

[2] Y. Ezoe, M. Muto, N. Uedo, "Magnifying narrowband imaging is more accurate than conventional white-light imaging in diagnosis of gastric mucosal cancer," Gastroenterology. 2011 Dec; 141(6):2017-2025

[3] J. Macqueen, "Some methods for Classification and analysis of multivariate observations," Proc. Fifth Berkeley Symp. on Math. Statist. and Prob., Vol. 1 (Univ. of Calif. Press, 1967), 281-297

[4] H. Yonggang, "Local Binary Pattern histogram based Texton learning for texture classification," 2011 18th IEEE International Conference on Image Processing, 841 - 844

[5] T. Ojala, "Multiresolution gray-scale and rotation invariant texture classification with local binary patterns," IEEE Transactions on Pattern Analysis and Machine Intelligence, 971 – 987, Jul 2002

[6] L. Mirmohamadsadeghi, A. Drygajlo, "Palm Vein Recognition with Local Binary Patterns and Local Derivative Patterns," International Joint Conference on Biometrics, Washington, DC, USA, October 10-13, 2011

[7] L. Nanni, A. Lumini, "A reliable method for cell phenotype image classification," Artif Intell Med. 2008 Jun; 43(2):87-97

[8] F. Riaz, F. B. Silva, M. D. Ribeiro, M. T. Coimbra, " Invariant Gabor texture descriptors for classification of gastroenterology images," IEEE Transactions on biomedical engineering, vol. 59, no. 10, October 2012

[9] K. Yao, G. K. Anagnostopoulos, K. Ragunath, "Magnifying endoscopy for diagnosing and delineating early gastric cancer," Endoscopy 2009; 41: 462–7.